Enzyme and Microbial Technology 95 (2016) 185–191

Contents lists available at ScienceDirect

Enzyme and Microbial Technology

journal homepage: www.elsevier.com/locate/emt

In vivo synthesis of nano-selenium by *Tetrahymena thermophila* SB210

Yin-Hua Cui[a,1], Ling-Li Li[a,1], Nan-Qing Zhou[a], Jing-Hua Liu[b], Qing Huang[b], Hui-Juan Wang[c], Jie Tian[c], Han-Qing Yu[a,*]

[a] CAS Key Laboratory of Urban Pollutant Conversion, Department of Chemistry, China
[b] Key Laboratory of Ion Beam Bioengineering, Hefei Institutes of Physical Science, Chinese Academy of Sciences, Hefei 230031, China
[c] Engineering and Materials Science Experiment Center, University of Science & Technology of China, Hefei 230026, China

ARTICLE INFO

Article history:
Received 21 March 2016
Received in revised form 6 August 2016
Accepted 27 August 2016
Available online 29 August 2016

Keywords:
Tetrahymena thermophila
Nano-selenium
Animal
Biosynthesis
Glutathione (GSH)
Proteins

ABSTRACT

Nano-selenium has a great potential to be used in chemical, biological, medical and environmental fields. Biological methods for nano-selenium synthesis have attracted wide interests, because they can be operated at ambient temperature and pressure without complicated equipments. In this work, a protozoa, *Tetrahymena thermophila (T. thermophila)* SB210, was used to *in vivo* synthesize nano-selenium. The biosynthesized nano-selenium was characterized using transmission electron microscopy, energy dispersive X-ray spectroscopy and Raman spectroscopy. The synthesized amorphous spherical selenium nanoparticles had diameters of 50–500 nm with the coexistence of irregular nano-selenium. The expressions of glutathione (GSH) synthesis related gene *glutathione synthase*, cysteine-rich protein metallothionein related gene *metallothionein-1* and [2Fe-2S] cluster-binding protein related gene were up-regulated in the nano-selenium producing group. Also, the subsequent GSH detection and *in vitro* synthesis experimental results suggest the three proteins were likely to be involved in the nano-selenium synthesis process.

1. Introduction

Nano-selenium is widely used due to its unique optical, spectral and other properties [1]. In biological and medical fields, nano-selenium has a great potential for practical applications. For example, nano-selenium showed an excellent antibacterial activity against *Staphylococcus aureus* compared with commercially available drug Ampicillin [2–4], and antifungal activity against several important clinical test strains [5]. In recent years, nano-selenium have been used for cancer therapy [6,7] and cancer-targeted nano-drug delivery [8]. Furthermore, nano-selenium also plays a positive role in wound healing, anti-oxidant and anti-Dengue virus [9].

To date, nano-selenium with desired sizes can be synthesized by chemical approaches [10], but they are usually expensive, environmentally contaminative, and require complicated equipments [11]. However, biological methods for nano-selenium synthesis are relatively simple, environmentally friendly and easier to be operated at ambient temperature and pressure [3]. Various types of organisms including bacteria [12,13], fungi [14] and plants [15] have been used for producing nano-selenium under mild conditions. Different species produced nano-selenium with distinct shapes and various sizes. However, there is no report about the synthesis of nano-selenium by animals yet.

Tetrahymena is a genus of protozoa, the simplest animals. It has cellular structural and functional complexity comparable to that of human [16], and has been proven to be a very valuable biological model in molecular biology, genetics [17–19] and toxicological studies [20]. Additionally, *Tetrahymena* has a rapid growth rate with a doubling time of less than two hours, which enables quick results and low maintenance costs [21]. These advantages make *Tetrahymena* an excellent surrogate model for animal research [22]. As a cost-effective animal, *Tetrahymena* is an ideal model to be explored for the synthesis of nano-selenium. The complete genome sequence of *T. thermophila* SB210 is available, enabling us to conduct mechanism studies on nano-selenium synthesis.

Therefore, in this work, nano-selenium was synthesized using *T. thermophila* SB210 in a simple, cost-effective and green way. Also, the prepared nano-selenium inside cells was characterized with various methods. Additionally, real-time polymerase chain reaction (PCR) and *in vitro* synthesis experiments were carried out to explore the underlying mechanism behind the nano-selenium synthesis in *Tetrahymena*.

* Corresponding author.
E-mail address: hqyu@ustc.edu.cn (H.-Q. Yu).
[1] These authors contributed equally to this work.

http://dx.doi.org/10.1016/j.enzmictec.2016.08.017
0141-0229/

Table 1
Primers for targeting genes.

Target gene	Primer sequence	Product size (bp)
Tubulin	Forward 5′-GTTCGGGAATGGG-3′ Reverse 5′-TTGAATAACTAGGAGCA-3′	396
Glutathione Synthase	Forward 5′-ATAAGAAGCAGGGTAG-3′ Reverse 5′-TCTCAAGGAAAGGGT-3′	215
mtt-1	Forward5′-GCGTAAGTAAGACTGATAAT-3′ Reverse 5′-AAGCAGCAGGGTTTAG-3′	145
2Fe2Sp	Forward 5′-CCACCATCATCACGC-3′ Reverse 5′-GCAGAAAGGACCATAAGT-3′	235

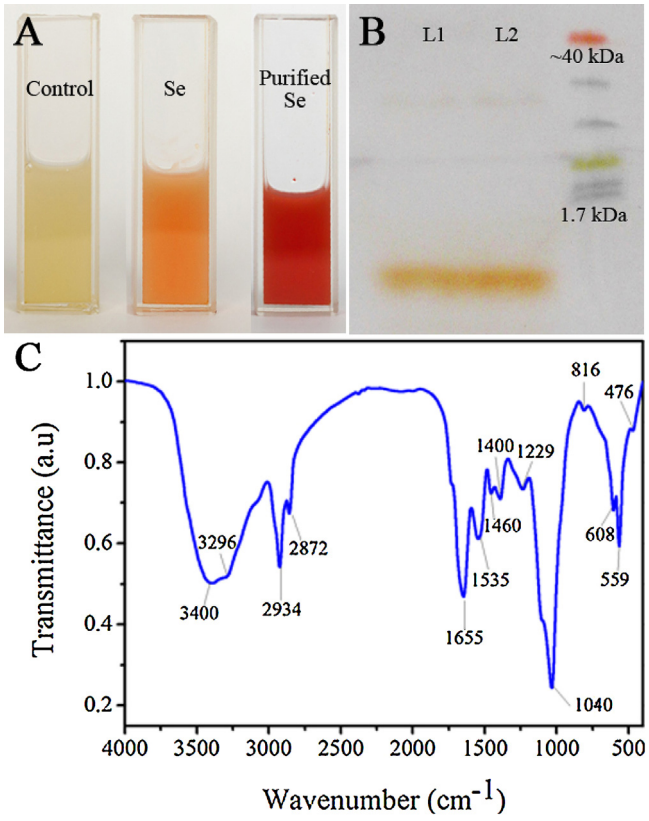

Fig. 1. Biosynthesis of the nano-selenium by *T. thermophila* SB210. (A) Control, selenite-dosing cells and purified nano-selenium; (B) SDS-PAGE electrophoresis of the purified nano-selenium; and (C) FTIR of purified nano-selenium.

2. Materials and methods

2.1. Nano-selenium synthesis and purification

T. thermophila (SB210) was kindly provided by Prof. Miao from the Institute of Hydrobiology, Chinese Academy of Sciences, China. The cells were grown in proteose peptone medium containing 1% (w/v) proteose peptone (BD, USA), 0.1% yeast extract (OXOID, UK), 0.2% glucose (Sinopharm Chemical Reagent Co., China), 0.003% ethylenediaminetetraacetic acid ferric sodium salt (Sigma-Aldrich, USA), and maintained at 27 °C in an orbital shaker (160 rpm).

When cells grew into the late log phase, 150 μM Na_2SeO_3 (Sigma-Aldrich, USA) was added into the medium. After additional 48-h cultivation, cells were centrifuged at 12,000 rpm for 5 min. The precipitate was washed twice with 10 mM Tris-HCl (pH 7.4) and re-suspended in the lysis buffer containing 2% (w/v) SDS (sodium dodecyl sulfate) and 0.2 M NaOH. Then, the cells were further treated by ultrasonic cell disruptor (Ningbo Scientz Biotechnology Co., China) for 10 min at a power output of 120 w in ice bath in order to release nano-selenium from cell components as much as possible. Finally, the homogenate was centrifuged at 12,000 rpm for

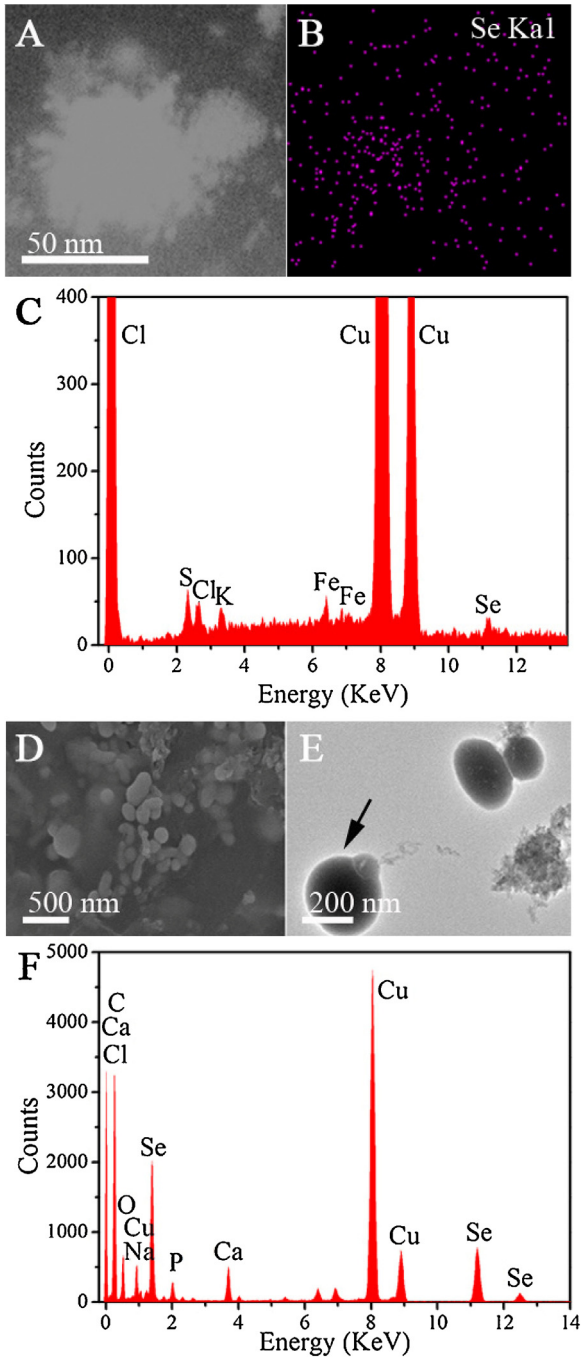

Fig. 2. Electron microscopy observation of the nano-selenium synthesized by *T. thermophila* SB210. (A) *In situ* dark-field electron microscopy; (B) corresponding Se element mapping of (A); (C) EDX of the nano-selenium; (D) SEM of the purified nano-selenium; (E) TEM of the purified nano-selenium; (F) EDX of purified nano-selenium indicated by arrow in (E).

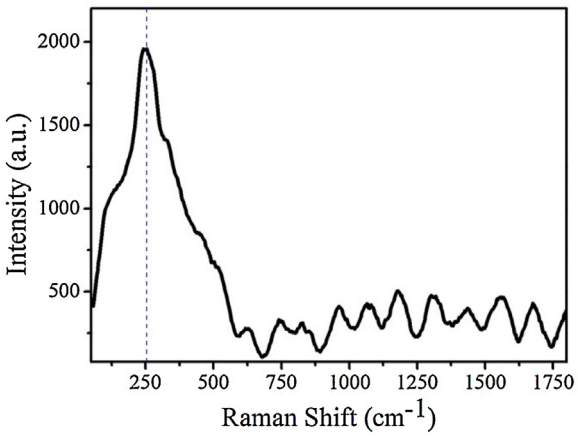

Fig. 3. Raman spectrum of the purified nano-selenium synthesized by *Tetrahymena*.

5 min to collect the precipitates, which contained nano-selenium and were washed more than three times with deionized water.

Inductively coupled plasma atomic emission spectrometry (ICP-AES, Thermo Jarrell Ash Co., USA) was used to determine the content of selenium. The samples were treated with 5 ml of nitric acid and heated until no more brown gas was produced and the solution containing nano-selenium turned colorless. After cooling the colorless solution to ambient temperature, hypochloric acid of 1.5 ml was added to the solution and heated to boil for several mins. After the treated samples were cooled to ambient temperature again, distilled water was added to set the volume to 5 ml.

2.2. SDS-polyacrylamide gel electrophoresis (SDS-PAGE) analysis

Purified nano-selenium samples were mixed with 5 × SDS-polyacrylamide gel electrophoresis (SDS-PAGE) loading buffer, which contained 250 mM Tris-HCl (pH 6.8), 10% SDS, and 50% glycerol (Sangon Biotech Co., China) without bromophenol blue. After adding 6% β-Mercaptoethanol (Amresco Co., USA) to solution, it was heated at 100 °C for 5 min. Then, the samples and Spectra Multicolor Low Range Protein Ladder (Thermo Scientific Inc., USA) were loaded onto a 12% SDS-PAGE. The gel was immediately electrophoresized at 120 V till the red band run to the bottom of the gel.

2.3. Characterization of nano-selenium

After 48-h cultivation with Na_2SeO_3, *T. thermophila* cells were centrifuged at 4000 rpm for 5 min and washed three times with 10 mM Tris-HCl (pH 7.4). Cells were fixed with 2.5% glutaraldehyde (Alfa Aesar, USA) for 2 h and dehydrated successively using 50%, 70%, 80%, 90%, 95% and 100% ethanol. Then, the cells were dropped on a copper grid with a carbon amorphous film, and dried under ambient conditions. The chemical composition of the samples was characterized by energy dispersive X-ray spectroscopy (EDX) and element mapping using scanning transmission electron microscope (STEM, JEM-ARM200F, JEOL Co., Japan). The morphology of the purified nano-selenium was observed by transmission electron microscope (TEM, JEM 2100F, JEOL Co., Japan) and scanning electron microscope (SEM, Supra 40, Zesiss Co., Germany). High-resolution transmission electron microscope (HRTEM) and selected area electron diffraction (SAED) patterns analyses were performed on the same TEM. Chemical composition of purified bio-selenium was characterized by EDX (AZtec X-MAX 80, Oxford Instruments, UK). Nano-selenium produced by glutathione (GSH) or cysteine *in vitro* was observed using TEM and analyzed using EDX.

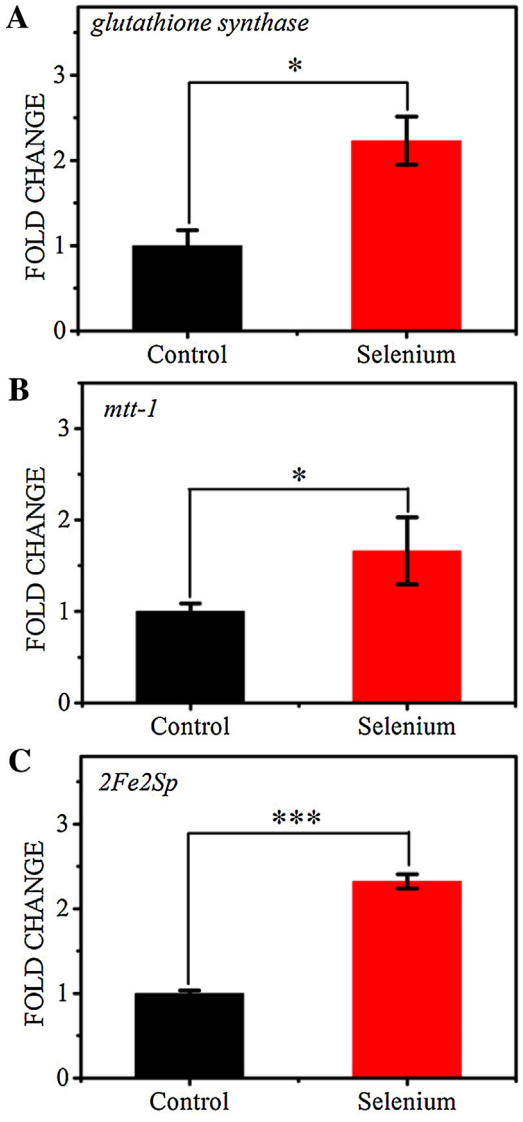

Fig. 4. Real-time PCR results of expression levels in the control and nano-selenium producing group. (A) *Glutathione synthase* gene, (B) *metallothionein-1*; and (C) *[2Fe-2S] cluster-binding protein*. Data are expressed as mean ± SE, $n = 3$. $^{*}p < 0.05$, $^{**}p < 0.01$, $^{***}p < 0.001$ compared to respective control.

Purified nano-selenium was diluted and put into quartz cuvettes of 1-cm width. The UV–vis spectroscopy analysis was performed on Aqualog (Horiba Co., Japan) in the spectral region of 240–600 nm.

Purified nano-selenium was dried by vacuum freeze dryer Free-Zone 2.5^{Plus} (LABCONCO, USA). The spectra was recorded by a Raman microspectrometer (XploRA, Horiba JobinYvon Co., France) equipped with a 532 nm laser and an Olympus 50 × long working distance lens.

The freeze dried, purified bio-selenium mixed with KBr was pressed into pellet for Fourier transform infrared (FTIR) detection. The spectrum was recorded on Vertex 70 (Bruker Co., Germany) at wavenumber range 4000–400 cm^{-1} with a resolution of 4.0 cm^{-1}. Atmosphere compensation, baseline correction and smoothing correction were performed on the FTIR spectra.

2.4. Real-time PCR analysis

Cells were collected and washed with 10 mM Tris-HCl (pH7.4). Total RNA of *Tetrahymena* cells of both control groups and nano-selenium producing group were extracted by RNAiso Plus (TAKARA

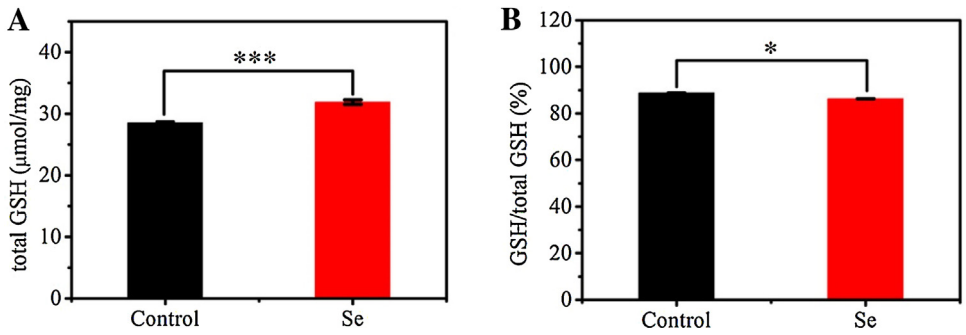

Fig. 5. GSH detection in the control and nano-selenium producing group. (A) The content of total GSH in cell mass; (B) Ratio of reduced GSH in total GSH. Data are expressed as mean ± SE, $n = 3$. $^{*}p < 0.05$, $^{**}p < 0.01$, $^{***}p < 0.001$ compared to respective control.

Co., Japan). Then, the total RNA was purified with Recombinant DNase I (Takara Co., Japan) under the protection of Recombinant RNase Inhibitor (Takara Co., Japan). Finally, total RNA was reversed to cDNA by PrimeScript RT reagent Kit Perfect Real Time (Takara Co., Japan). Real-time PCR was performed using SYBR Premix Ex Taq™ II (Takara Co., Japan) on Step One™ Real-Time PCR System (Life Technologies, USA). Cysteine-rich proteins related genes, *glutathione synthase*, *metallothionein-1* (*mtt-1*) *and* [*2Fe-2S*] *cluster-binding protein* (*2Fe2Sp*), were tested. The gene-specific primers are described in Table 1 with *tubulin* as the control. Fold change was normalized to control group. Test for each sample was repeated three times and three independent tests were operated.

2.5. GSH detection

The control and nano-selenium-producing *Tetrahymena* cells were collected by centrifugation and washed with 1 × PBS (phosphate-buffered saline). The GSH and GSSG (oxidized GSH) were detected following the protocol of GSH and GSSG Detection Assay Kit (Beyotime Biotechnology Co., China). Total protein content of each sample was determined by BCA Protein Assay Kit (Sangon Biotech Co., China).

2.6. In vitro *synthesis test*

Glutathione and cysteine were resolved in 1 × PBS to the final concentration of 1 mM separately. 150 μM Na_2SeO_3 was added to the solution and both the systems reacted at 27 °C for 15 min until they turned red. Then, the two solutions were dried by vacuum freeze dryer to concentrate nano-selenium and dropped on copper grids for TEM observation.

2.7. Statistical analysis

Mean values and standard errors of gene expressions were calculated and analysis of variances was carried out with Microsoft Office Excel 2007. The *P* values less than 0.05 were considered statistically significant.

3. Results and discussion

3.1. In vivo *biosynthesis of nano-selenium*

T. thermophila was cultivated in the medium containing selenite when it grew into late log phase toform nano-selenium. The whole medium turned red slightly after being incubated with selenite, but the control group did not show such a color change. The selenite concentration was optimized by treating the cells with different concentrations of selenite for 48 h. As shown in Fig. S1A, the homogenate of the 150-μM-dosed group was much redder than the homogenate of the 100-μM-dosed group. The protozoa treated with 150 μM selenite exhibited the highest nano-selenium yield and 150 μM selenite was selected in the subsequent experiments (Fig. S1A). As for the time optimization, the homogenate exhibited no big difference in color between the 48-h and 72-h treatments. Thus, 48 h was chosen as the incubation time in the subsequent experiments (Fig. S1B). When *Tetrahymena* was treated with 150 μM selenite and incubated for 48 h, the homogenate color of the selenite-dosed group was obviously more red than that of the control group, and the further purification and concentration made it much more red (Fig. 1A). The purified red materials were loaded in Lane 1 and Lane 2 of the SDS-PAGE gel and protein ladder was loaded in the last lane. The electrophoresis result shows that the nano-selenium was attached to the biomolecules. FTIR analytical result confirms the binding of the nano-selenium with proteins (Fig. 1C). Peaks of O—H, C—H, Amide I (1655 cm^{-1}), Amide II (1535 cm^{-1}), C—O—C (1040 cm^{-1}) were obtained from the bio-selenium spectrum [23], indicating the presence of proteins and carbohydrates on the purified bio-selenium, which is consistent with the SDS-PAGE results. Nano-selenium produced by bacteria, fungi and plant extracts also exhibites interactions with proteins and other biomolecules [24,25]. Proteins that adhere to nano-selenium might stabilize it in their formation or might act as a capping agent to control the size of nano-selenium [26]. Furthermore, these proteins may increase biological activity of nano-selenium [9]. In addition to proteins, carbohydrates can also act as “template” for nano-selenium nucleation and control its shape and size [26].

3.2. Characteristics of the synthesized nano-selenium

To verify the generation of nano-selenium in *T. thermophila*, several methods were used to characterize the red materials mentioned above. Firstly, STEM was used to explore the cells exposed to selenite (Fig. 2). Dark-field image shows that the materials produced in *T. thermophila* were anisotropic particles with small sizes (Fig. 2A). Fig. 2C shows their EDX microanalytical results. Presence of Se peaks confirmed the production of nano-selenium. The strong absorption peaks of copper were attributed to the TEM supporting copper grid, while the iron, sulfur, chlorine and potassium should be associated with the biomolecules like proteins. The corresponding Se element mapping of Fig. 2A further confirm the formation of nano-selenium (Fig. 2B). The STEM, element mapping and EDX results are consistent with each other, indicating the formation of nano-selenium. Detailed properties of the purified nano-selenium were further investigated using electron microscopes. Various sizes of nano-selenium were observed with SEM (Fig. 2D) and TEM (Fig. 2E). Despite of the absorptions of carbon, copper and other elements that were from the TEM supporting grid and organic biomolecules, the EDX exhibited very strong

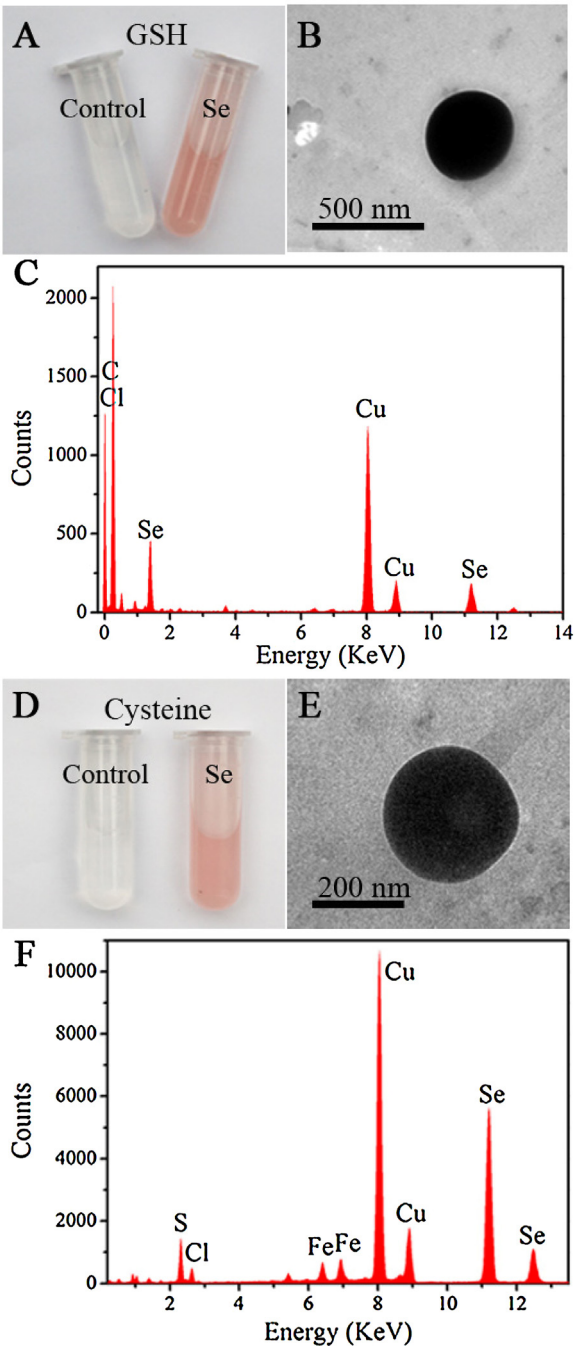

Fig. 6. *In vitro* synthesis experimental results. (A) Control (left) and selenite-adding (right) group of GSH; (B) TEM of selenium nanoparticles produced by GSH; (C) EDX of selenium nanoparticles produced by GSH; (D) Control (left) and selenite-adding (right) group of cysteine; (E) TEM of selenium nanoparticles produced by cysteine; and (F) EDX of selenium nanoparticles produced by cysteine.

absorption of selenium, indicating that the purified material was bio-selenium (Fig. 2F). The crystal structure of the purified nano-selenium was examined by HRTEM and SAED, which show that the nano-selenium synthesized by *Tetrahymena* was amorphous (Fig. S2). Diameters of the most amorphous selenium nanoparticles were in a range of 50–500 nm and the length of the irregular nano-selenium was less than 1 μm. 120 nano-selenium particles were observed using TEM. Among them, 27.5% nano-selenium had irregular shape with length less than 500 nm and width not less than 50 nm. The rest were selenium nanoparticles. As shown in Fig. S3, the diameters of most of them were less than 200 nm. The size of the selenium nanoparticles is of a similar level to those produced by aerobic and anaerobic bacteria reported previously [26].

As for the irregular nano-selenium, a similar phenomenon was reported by Gates et al. [27]. In their work, in the absence of stabilizing ligand, amorphous selenium became aggregated, resulting in the irregular nanoparticles in the nano-selenium formation process. Other species like *Bacillus megaterium* and *Pseudomonas alcaliphila* also produced nano-selenium with similar morphology to the nano-selenium synthesized by *Tetrahymena* [28,29]. However, these species formed crystalline nano-selenium or nanorods [28,29]. An important step of forming nanorods is that the selenium should precipitate as nanocrystallites of t-Se [27]. The reason why *Tetrahymena* did not produce crystalline nano-selenium like other species might be attributed to the low concentration of selenite used in our work. Obviously, further modification of the biosynthesis method is needed to control the shape and size of the nano-selenium formed in *T. thermophila* SB210.

Raman spectroscopic analysis of the purified materials was used to confirm the synthesis of nano-selenium by *T. thermophila*. As shown in Fig. 3A, a peak at 254 cm^{-1} was observed, which is consistent with the specific Raman peak of amorphous nano-selenium, instead of trigonal selenium, whose peak is located at 234 cm^{-1} [30]. The above characterization results demonstrate the formation of nano-selenium in *T. thermophila* SB210.

3.3. Mechanism of nano-selenium formation by T. thermophila

Thiol-containing compounds play important roles in many biochemical reactions because they are oxidized and regenerated readily [31]. They are involved in the detoxification of cellular stresses including metals [32] and reactive oxygen stress (ROS) [33]. GSH, as the most abundant thiol (SH) found in the eukaryotic cells, presents at concentrations up to 12 mM in mammalian cells [34], and is suspected to be involved in selenium metabolism [35]. The RNA detections of the suspected genes were performed by real-time PCR to uncover the mechanism of selenite reduction in *T. thermophila*. Glutathione synthase expressed by *glutathione synthase* gene is one of the enzymes that catalyze the GSH formation reactions [36]. As shown in Fig. 4A, mRNA expression level of glutathione synthase was enhanced in the nano-selenium forming group compared with the control group. This result suggests that GSH might play an important role in the selenite reduction process. Considering that thiol of GSH is from amino acid cysteine, cysteine-rich proteins related genes *metallothionein-1* and [*2Fe-2S*] *cluster-binding protein* were also detected. Metallothioneins are small cysteine-rich proteins, which always play detoxification roles in cells through binding heavy metals [32]. [2Fe-2S] cluster binding protein possesses a cysteine-rich center, which can coordinate with iron and sulfide ions [37]. Both of them were also up-regulated in the nano-selenium forming group compared with the control group (Fig. 4B and C). The over expressed metallothioneins and [2Fe-2S] cluster-binding proteins might be also involved in the reduction of selenite to nano-selenium.

The real-time PCR result was further confirmed by the GSH detection. Total content of GSH increased in the selenium-producing group compared to the control (Fig. 5A). The increased expression of *glutathione synthase* gene resulted in the elevation of GSH in cells. As for the ratio of GSH/total GSH, a slight decrease was observed in the nano-selenium-producing group (Fig. 5B). The reason for this reduction might be the fast consumption of GSH in the nano-selenium producing process.

In order to confirm the roles of the expressed GSH and the cysteine-rich proteins in reducing selenite to nano-selenium, *in vitro* experiment was conducted. The solution turned red after adding selenite into 1 mM GSH, compared with control group (Fig. 6A), and the red color was similar to that of the nano-selenium

synthesized using *Tetrahymena* (Fig. 1). This solution was directly loaded onto copper gird for TEM observation. Well dispersed spherical nanoparticles, which are similar to those in Fig. 2E, were observed (Fig. 6B). The diameters of most of these particles were in a range of 50–500 nm, which are also similar to those of the selenium nanospheres synthesized by *Tetrahymena*. However, irregular nano-selenium was not found in this case. This difference between the *in vivo* and *in vitro* produced nano-selenium might be attributed to the complexity of living organisms. Instead in the *in vitro* system, GSH might stabilize the nano-selenium and prevent it from aggregating and rupturing into irregular shapes. However, some of the *in vivo* synthesized nano-selenium might not be stabilized by any ligand. As shown in Fig. 6C, strong Se absorption peaks were detected by EDX. Peaks of chlorine should be from GSH and PBS in solution, while strong absorption peaks of copper and carbon belonged to the copper grid. The TEM and EDX results verify the formation of nano-selenium by GSH, suggesting that GSH had the ability of reducing selenite into nano-selenium.

Similar results were obtained when selenite was added into 1 mM cysteine (Fig. 6D–F). Spherical selenium particles synthesized using cysteine were relatively larger than the above two samples, suggesting that various sizes of nano-selenium produced by *Tetrahymena* might be attributed to different synthesis mechanisms. The diameter of the largest one exceeded 900 nm, but no irregular nano-selenium was observed in the GSH system. Also, carbon, oxygen, sodium, sulfur, chlorine (elements of cysteine and PBS) and iron, copper (from the TEM supporting grid) were detected (Fig. 6F). These results demonstrate the formation of nano-selenium using cysteine and the reduction ability of cysteine. Real-time PCR, GSH detection and the *in vitro* synthesis experiments suggest that GSH and cysteine-rich proteins were involved in the synthesis of nano-selenium by *T. thermophila* SB210.

4. Conclusions

In this work a simple, cost-effective and eco-friendly method for synthesizing nano-selenium using *T. thermophila* SB210 was developed. Red spherical selenium nanoparticles with diameters of 50–500 nm were synthesized *in vivo*, as demonstrated by the electron microscopy, energy dispersive X-ray spectroscopy and Raman spectroscopy results. The real-time PCR, GSH detection and *in vitro* synthesis experimental results indicate that GSH and the cysteine-rich proteins could reduce selenite into nano-selenium and that the three proteins were likely to be involved in the nano-selenium synthesis process. *Tetrahymena thermophila*, a protozoa, was demonstrated to be efficient in the synthesis of nano-selenium.

Acknowledgements

The work was supported by the Natural Science Foundation of China (21477120), and the Collaborative Innovation Center of Suzhou Nano Science and Technology of the Ministry of Education of China. Prof. Wei Miao from the Institute of Hydrobiology, Chinese Academy of Sciences, China is acknowledged for his kind provision of *Tetrahymena thermophila* SB210.

Appendix A. Supplementary data

Supplementary data associated with this article can be found, in the online version, at http://dx.doi.org/10.1016/j.enzmictec.2016.08.017.

References

[1] T.W. Smith, R.A. Cheatham, Functional polymers in the generation of colloidal dispersions of amorphous selenium, Macromolecules 13 (1980) 1203–1207.
[2] N. Srivastava, M. Mukhopadhyay, Green synthesis and structural characterization of selenium nanoparticles and assessment of their antimicrobial property, Bioprocess Biosyst. Eng. 38 (2015) 1723–1730.
[3] E. Zonaro, S. Lampis, R.J. Turner, S.J.S. Qazi, G. Vallini, Biogenic selenium and tellurium nanoparticles synthesized by environmental microbial isolates efficaciously inhibit bacterial planktonic cultures and biofilms, Front. Microbiol. 6 (2015).
[4] V. Bartůněk, J. Junková, J. Šuman, K. Kolářová, S. Rimpelová, P. Ulbrich, et al., Preparation of amorphous antimicrobial selenium nanoparticles stabilized by odor suppressing surfactant polysorbate 20, Mater. Lett. 152 (2015) 207–209.
[5] A.R. Shahverdi, A. Fakhimi, G. Mosavat, P. Jafari-Fesharaki, S. Rezaie, S.M. Rezayat, Antifungal activity of biogenic selenium nanoparticles, World Appl. Sci. J. 10 (2010) 918–922.
[6] P. Tran, T.J. Webster, Novel anti-cancer orthopedic materials: nanostructured selenium, Bioeng. Conf. 2007. NEBC'07. IEEE 33rd Annu. Northeast, IEEE (2007) 241–242.
[7] Y. Wang, P. Chen, G. Zhao, K. Sun, D. Li, X. Wan, et al., Inverse relationship between elemental selenium nanoparticle size and inhibition of cancer cell growth *in vitro* and *in vivo*, Food Chem. Toxicol. 85 (2015) 71–77.
[8] T. Liu, L. Zeng, W. Jiang, Y. Fu, W. Zheng, T. Chen, Rational design of cancer-targeted selenium nanoparticles to antagonize multidrug resistance in cancer cells, Nanomed. Nanotechnol. Biol. Med. 11 (2015) 947–958.
[9] S. Ramya, T. Shanmugasundaram, R. Balagurunathan, Biomedical potential of actinobacterially synthesized selenium nanoparticles with special reference to anti-biofilm anti-oxidant, wound healing, cytotoxic and anti-viral activities, J. Trace Elem. Med. Biol. 32 (2015) 30–39.
[10] N.C. Johnson, S. Manchester, L. Sarin, Y. Gao, I. Kulaots, R.H. Hurt, Mercury vapor release from broken compact fluorescent lamps and in situ capture by new nanomaterial sorbents, Environ. Sci. Technol. 42 (2008) 5772–5778.
[11] B. Langi, C. Shah, K. Singh, A. Chaskar, M. Kumar, P.N. Bajaj, Ionic liquid-induced synthesis of selenium nanoparticles, Mater. Res. Bull. 45 (2010) 668–671.
[12] M. Kuroda, E. Notaguchi, A. Sato, M. Yoshioka, A. Hasegawa, T. Kagami, et al., Characterization of *Pseudomonas stutzeri* NT-I capable of removing soluble selenium from the aqueous phase under aerobic conditions, J. Biosci. Bioeng. 112 (2011) 259–264.
[13] K. Tam, C.T. Ho, J.-H. Lee, M. Lai, C.H. Chang, Y. Rheem, et al., Growth mechanism of amorphous selenium nanoparticles synthesized by *Shewanella sp*. HN-41, Biosci. Biotechnol. Biochem. 74 (2010) 696–700.
[14] E. Vetchinkina, E. Loshchinina, V. Kursky, V. Nikitina, Reduction of organic and inorganic selenium compounds by the edible medicinal basidiomycete *Lentinula edodes* and the accumulation of elemental selenium nanoparticles in its mycelium, J. Microbiol. 51 (2013) 829–835.
[15] T. Chen, Y.-S. Wong, W. Zheng, Y. Bai, L. Huang, Selenium nanoparticles fabricated in *Undaria pinnatifida* polysaccharide solutions induce mitochondria-mediated apoptosis in A375 human melanoma cells, Colloids Surf. B Biointerfaces 67 (2008) 26–31.
[16] M.-C. Yao, J.-L. Chao, C.-Y. Cheng, Programmed genome rearrangements in tetrahymena, Microbiol. Spectr. 2 (2014).
[17] K. Collins, R. Kobayashi, C.W. Greider, Purification of *Tetrahymena* telomerase and cloning of genes encoding the two protein components of the enzyme, Cell 81 (1995) 677–686.
[18] E. Orias, Probable somatic DNA rearrangements in mating type determination in *Tetrahymena thermophila*: a review and a model, Dev. Genet. 2 (1981) 185–202.
[19] T.R. Cech, Self-splicing and enzymatic activity of an intervening sequence RNA from *Tetrahymena*, Biosci. Rep. 24 (2004) 362–385.
[20] W. Li, H. Li, J. Zhang, X. Tian, Effect of melamine toxicity on *Tetrahymena thermophila* proliferation and metallothionein expression, Food Chem. Toxicol. 80 (2015) 1–6.
[21] D.M. Cassidy-Hanley, *Tetrahymena* in the laboratory: strain resources, methods for culture, maintenance, and storage, Methods Cell Biol. 109 (2012) 237.
[22] N.P. Sauvant, D. Pepin, E. Piccinni, *Tetrahymena pyriformis*: a tool for toxicological studies. A review, Chemosphere 38 (1999) 1631–1669.
[23] R. Jain, N. Jordan, S. Weiss, H. Foerstendorf, K. Heim, R. Kacker, et al., Extracellular polymeric substances govern the surface charge of biogenic elemental selenium nanoparticles, Environ. Sci. Technol. 49 (2015) 1713–1720.
[24] L. Zhang, D. Li, P. Gao, Expulsion of selenium/protein nanoparticles through vesicle-like structures by *Saccharomyces cerevisiae* under microaerophilic environment, World J. Microbiol. Biotechnol. 28 (2012) 3381–3386.
[25] A. Husen, K.S. Siddiqi, Plants and microbes assisted selenium nanoparticles: characterization and application, J. Nanobiotechnol. 12 (2014) 28.
[26] R. Jain, G. Gonzalez-Gil, V. Singh, E.D. Van Hullebusch, F. Farges, P.N.L. Lens, Biogenic selenium nanoparticles: production, characterization and challenges, in: Nanobiotechnology, Stud. Press LLC, USA, 2014, pp. 361–390.
[27] B. Gates, B. Mayers, B. Cattle, Y. Xia, Synthesis and characterization of uniform nanowires of trigonal selenium, Adv. Funct. Mater. 12 (2002) 219.
[28] W. Zhang, Z. Chen, H. Liu, L. Zhang, P. Gao, D. Li, Biosynthesis and structural characteristics of selenium nanoparticles by *Pseudomonas alcaliphila*, Colloids Surf. B Biointerfaces 88 (2011) 196–201.
[29] R.R. Mishra, S. Prajapati, J. Das, T.K. Dangar, N. Das, H. Thatoi, Reduction of selenite to red elemental selenium by moderately halotolerant *Bacillus megaterium* strains isolated from Bhitarkanika mangrove soil and characterization of reduced product, Chemosphere 84 (2011) 1231–1237.

[30] A.J. Kora, L. Rastogi, Biomimetic synthesis of selenium nanoparticles by *Pseudomonas aeruginosa* ATCC 27853: an approach for conversion of selenite, J. Environ. Manage. 181 (2016) 231–236.
[31] D.A. Dickinson, H.J. Forman, Cellular glutathione and thiols metabolism, Biochem. Pharmacol. 64 (2002) 1019–1026.
[32] C. Cobbett, P. Goldsbrough, Phytochelatins and metallothioneins: roles in heavy metal detoxification and homeostasis, Annu. Rev. Plant Biol. 53 (2002) 159–182.
[33] C.K. Sen, L. Packer, Antioxidant and redox regulation of gene transcription, FASEB J. 10 (1996) 709–720.
[34] R. Dringen, Metabolism and functions of glutathione in brain, Prog. Neurobiol. 62 (2000) 649–671.
[35] J. Kessi, K.W. Hanselmann, Similarities between the abiotic reduction of selenite with glutathione and the dissimilatory reaction mediated by *Rhodospirillum rubrum* and *Escherichia coli*, J. Biol. Chem. 279 (2004) 50662–50669.
[36] Y. Li, R. Cui, P. Zhang, B.-B. Chen, Z.-Q. Tian, L. Li, et al., Mechanism-oriented controllability of intracellular quantum dots formation: the role of glutathione metabolic pathway, ACS Nano. 7 (2013) 2240–2248.
[37] S. Tamir, Y. Eisenberg-Domovich, A.R. Conlan, J.T. Stofleth, C.H. Lipper, M.L. Paddock, et al., A point mutation in the [2Fe?2S] cluster binding region of the NAF-1 protein (H114C) dramatically hinders the cluster donor properties, Acta Crystallogr. Sect. D Biol. Crystallogr. 70 (2014) 1572–1578.